Preprints.org

Article

Not peer-reviewed version

Surface Behavior of ZnO Films Prepared at Room Temperature

Da-Hua Wei *, Sheng-Kai Tong , Sheng-Chiang Chen , Rong-Tan Huang *

Posted Date: 12 July 2023

doi: 10.20944/preprints202307.0833.v1

Keywords: surface behavior; internal stress; ultraviolet light power; photocatalytic; heterostructure

Preprints.org is a free multidiscipline platform providing preprint service that is dedicated to making early versions of research outputs permanently available and citable. Preprints posted at Preprints.org appear in Web of Science, Crossref, Google Scholar, Scilit, Europe PMC.

Copyright: This is an open access article distributed under the Creative Commons Attribution License which permits unrestricted use, distribution, and reproduction in any medium, provided the original work is properly cited.

Preprints (www.preprints.org) | NOT PEER-REVIEWED | Posted: 12 July 2023 doi:10.20944/preprints202307.0833.v1

Disclaimer/Publisher's Note: The statements, opinions, and data contained in all publications are solely those of the individual author(s) and contributor(s) and not of MDPI and/or the editor(s). MDPI and/or the editor(s) disclaim responsibility for any injury to people or property resulting from any ideas, methods, instructions, or products referred to in the content.

Article

Surface Behavior of ZnO Films Prepared at Room Temperature

Da-Hua Wei [1,*], Sheng-Kai Tong [2], Sheng-Chiang Chen [1] and Rong-Tan Huang [3,*]

[1] Institute of Manufacturing Technology, Department of Mechanical Engineering, National Taipei University of Technology (TAIPEI TECH), Taipei 10608, Taiwan; synder@ms6.hinet.net (S.-C.C.)
[2] Research and Development Department, CB-CERATIZIT Group, New Taipei City 24250, Taiwan; mmm.ntut@gmail.com
[3] Department of Optoelectronics and Materials Technology, National Taiwan Ocean University, Keelung 20224, Taiwan
* Correspondence: dhwei@ntut.edu.tw (D.-H.W.); rthuang@mail.ntou.edu.tw (R.-T.H.)

Abstract: The surface behavior of the ZnO[-based films could be modulated via a postannealing and ultraviolet (UV) irradiation with different powers and time, respectively. These present results could provide modulate the microstructure related in grain-size distribution and photocatalytic behavior for potential guide in the field of wide bandgap semiconducting oxides. The ZnO films were prepared onto Corning-1737 glass substrates by using radio-frequency magnetron sputtering without supplying oxygen source at room temperature. For the purpose of obtaining modulable grain microstructures, the as-prepared ZnO films (Z0) were treated via a postannealing modification in vacuum furnace at 300°C for 30 *minutes* after deposition (Z300) accompanied with the adjustable internal stress. The contact angle (CA) value of ZnO film reduced from 95° to 68° was owning to the different grain microstructure accompanied by a change in size variation. In addition, the UV light with different irradiation powers could also be used to improve the hydrophilicity varied from hydrophobic status to superhydrophilic status due to the desirable surface characteristics of the **photocatalytic** action. In addition, the photocatalytic activity of ZnO film exhibited efficient photodegradation of methylene blue (MB) under UV irradiation, with a chemical reaction constant of 2.93×10^{-3} min^{-1}. In this present work, we demonstrated that the CA value of the ZnO films not only caused from hydrophobic to hydrophilic status accompanied by a change in grain size combined with internal stress but also induced by the UV light irradiation combined with photocatalytic activity simultaneously. On the other hand, the enhanced surface plasmonic resonance could be observed that is due to couple electron and photon oscillations and can be generated at the interface between a flat, continuous Pt capping nanolayer. This designed structure could also be considered as a Pt electrode pattern onto ZnO (metal Pt/ ceramic ZnO) for multifunctional heterostructured sensors and devices in near future.

Keywords: surface behavior; internal stress; ultraviolet light power; photocatalytic; heterostructure

1. Introduction

The surface behavior of oxide materials has been considered for various powerful applications including sensors, detectors, cleanup of the environment, energy conversion and related memory nanodevices [1–12]. The various sensors and detectors have been focused and developed on one-dimensional (1-D) nanostructures and existed difficult task for super large-scale manufacture with uniformity. The functional coatings deposited on metal, ceramics, semiconductor, and corresponded nanostructures are easy and useful way to obtain significantly surface plasmonic enhancement in the electrical and optical performances combined with bottom materials [13–17]. So the strong plasmon-exciton coupling in metallic capping shell combined with semiconductor-based materials has potentially provided a method to enhance the plasmon-exciton interaction and corresponded specificity for many application areas [18–20]. The hydrophobic/ hydrophilic functional coatings are

© 2023 by the author(s). Distributed under a Creative Commons CC BY license.

Preprints (www.preprints.org) | NOT PEER-REVIEWED | Posted: 12 July 2023 doi:10.20944/preprints202307.0833.v1

usually fabricated by modulating surface status with low/ high surface energy for generating nano/ micro structures. The zinc oxide (ZnO) is easier to form texture with the lowest surface energy at (002) plane, also, ZnO is a general material for photocatalysis among the metal oxides. ZnO compound displays a photo *reactivity* under ultraviolet (UV) light irradiation owning to its wide band gap, and its surface wetting state could be modulated significantly by irradiation strength with a light energy of UV [21–25]. Therefore, the semiconducting ZnO compound is a suitable selection for multifunctional surface coating. A reversible UV light-driven hydrophobic/ hydrophilic surface characteristic for ZnO-based nanostructures and related nano- wires/ rods decorated with metallic nanoparticles has been widely developed and demonstrated [26–29].

The semiconducting ZnO compound has typical large exciton binding energy (60 meV), direct wide-bandgap (3.37 eV) and highly transparent in the visible region with a transmittance of over 80%. Hence this is an excellent selection for future potential applications and used in UV detectors, light emitters, transparent thin film transistors, solar cells, piezoelectric transducers, chemical gas sensors, biosensors, and resistive random-access memory (RRAM) devices [30–35]. Owning to the various potential applications, ZnO has a modulational effect of surface characteristics, which can offer a remarkable *surface* behavior including photocatalytic activity and reversible hydrophobic/ hydrophilic wetting *transition* by using UV light irradiation originated from its intrinsic semiconducting characteristics. It can be known that the reversible wettability and modulation of ZnO compound was due to the competition of surface chemical *characteristics* between adsorption and desorption of rearrangement of hydroxyl groups and organic supply chains on its surface status [36,37]. One of the photo *reactive* materials such as ZnO has been highly applied its surface characteristics and used to display modulated wetting behavior combined a quickly hydrophobic/ hydrophilic transition with modulational contact angles. The various methods have been claimed on controlling surface microstructures, which are developed to modulate the wetting and photocatalytic behavior of functional coatings. On the other hand, the different grown skills of ZnO hetroepitaxy films have been reported [38–46], the sputtering coating skill is a suitable one for manufacturing large-area uniform ZnO films for the purpose of applying for future cleanup of the environment, related optoelectronic nanodevices and biosensors because it has received an important attention due to its stable deposition rates and with rapid growth of high-quality coatings at low temperature. It can be understood that the deposited uniformity of nanostructures, thin, and thick films with super large area was caused by various sputtering specifications including sputtering power, sputtering pressure, supplying content gas, substrate temperature, and the distance between target and substrate.

In our present work, the surface behavior of highly textured ZnO films prepared by using RF sputtering system without supplying oxygen source at room temperature have been investigated. The wetting behavior, grain size, and morphological features on the surface of textured ZnO films were modulated via a direct postannealing modification. The transmittance for all textured ZnO films was also examined and demonstrated. The surface wetting behavior of textured ZnO films was checked by water contact angle measurement equipment. The modulable wetting behavior was obtained by adjusting the strength of UV light irradiation and storage in dark room for 12 hrs to reach the initial water contact angle. Our claimed work also offers a simple skill to modulate the wetting behavior of ZnO films by modulating UV power density. The coupling of surface plasmons and excitons using a continuous Pt capping nanolayer onto ZnO film has been selected to study the coupling effect for the metal/ semiconducting oxide heterostructures, and could be used for the fabrication of nanodevices in next step. Our claimed work presented a convenient and original method to modulate surface behavior and enhance surface plasmons for wide-bandgap semiconducting ZnO just directly by capping a metallic nanolayer not such as to decorate with metallic nanoparticles. This not only enlarges the future requirements of ZnO compound but also power-assists a simple idea with wide-bandgap semiconducting material sketch and nanodevice evolution on *flexible and transparent* substrates for future wearable technologies.

Preprints (www.preprints.org) | NOT PEER-REVIEWED | Posted: 12 July 2023 doi:10.20944/preprints202307.0833.v1

2. Experiments and Film Structures

The textured ZnO films were prepared onto Corning-1737 glass substrates by using radio-frequency (RF) magnetron sputtering without supplying oxygen source at room temperature. The glass substrates in chamber have been placed parallel to ZnO binary target with 99.99% purity, whose thickness and diameter are 3 mm and 51 mm, respectively. The glass substrates were cleaned in acetone and ethanol at first to withdraw organic contaminants, then ultrasonically rinsed in deionized water, and finally dried in hot air before set the glass substrates into the working chamber. The high vacuum working chamber was pumped down to a base pressure of 4.5×10^{-7} torr. The argon gas was then used in working chamber with a working pressure of 1×10^{-2} torr and without supplying oxygen gas. The ZnO films have been prepared using 75 W RF power, and all the film thickness was fixed at 250 nm. Furthermore, for the purpose of obtaining modulable grain microstructures, one of the as-prepared ZnO sample was during postannealing modification in furnace at 300°C for 30 *minutes* after deposition.

The crystalline preferred orientation and crystallinity in ZnO films was examined by X-ray diffraction analysis (XRD, PANalytical, Almelo, The Netherlands) with Cu Kα radiation (λ = 1.54 Å) in the 2θ ranges of 20–90°. The morphological features on the surface and corresponding elemental information for ZnO films was performed by scanning electron microscope (SEM, Phenom XL G2, Thermo Scientific, Massachusetts, USA) and field emission scanning electron microscopy (FE-SEM, Dresden, Germany), respectively. The chemical composition of the ZnO compound was identified to be $Zn_{40}O_{60}$ by field emission electron probe X-ray microanalysis (FE-EPMA, JEOL, Tokyo, Japan). The measurement and calculation for contact angle and surface free energy of ZnO films was evaluated with the water contact angle (CA, Rame-Hart 100 goniometer, **Capovani Brothers Inc.,** NY, USA) measurement by using small drop of liquid water onto surface for individual ZnO sample. The degree of accuracy for the water contact-angle measurement was induced by the image quality, using a charge-coupled device (CCD) to capture the images of the drop of liquid water (~ 5 μL). And then the processing of the fitting curve function was achieved immediately by using CA software, and the value was evaluated to be about ±1 degree. In addition, the related measurement of surface free energy (SFE) for individual sample was also simultaneously evaluated. The power energy of ultraviolet (UV) light irradiated with ZnO films was between 330 and 3330 mW/cm^2 by using mercury arc lamp (HAMAMATSU-Deuterium L2D2) with a 365 nm wavelength. In this work, the as-prepared ZnO films without any postannealing modification and with a 300°C postannealing modification will be denoted below as Z0 and Z300, respectively.

3. Results and Discussion

The X-ray diffraction spectra for the samples Z0 and Z300 are shown in Figure 1(a). The XRD spectra confirm both samples demonstrate a tough peak positioned at approximately 2θ = 34°, which is corresponded to the high degree of *c*-axis orientation with wurtzite crystal structure along ZnO (002) plane (JCPDS Card: 36-1451). The large intensity of the diffraction spectra originated from the ZnO (002) plane is owing to the smallest surface energy in the ZnO (002) basal plane in wurtzite crystal structure, contributing to a crystallographic orientation along the [001] preferred crystalline direction. The peak intensity of ZnO (002) diffraction angle enhanced considerably with increasing the temperature and time of postannealing modification, which is due to much more energy to improve the crystallinity via a postannealing process. In addition, from the XRD spectrum of sample Z300, there is still have one slight peak located at around 76.6°, *indexing as* ZnO (004). It can be known that without any peaks except the (00n) diffraction angles are obtained over a large angular range (θ–2θ scan), demonstrating the ZnO film did epitaxially prepare onto the glass substrates. In addition, as shown in Figure 1(b), it can also be demonstrated that the ZnO (002) diffraction peak slightly changed from low angle region (2θ = 34.36°) toward high angle region (2θ = 34.39°), indicating the internal stress of the ZnO films have been modulated via a direct postannealing modification.

Preprints (www.preprints.org) | NOT PEER-REVIEWED | Posted: 12 July 2023 doi:10.20944/preprints202307.0833.v1

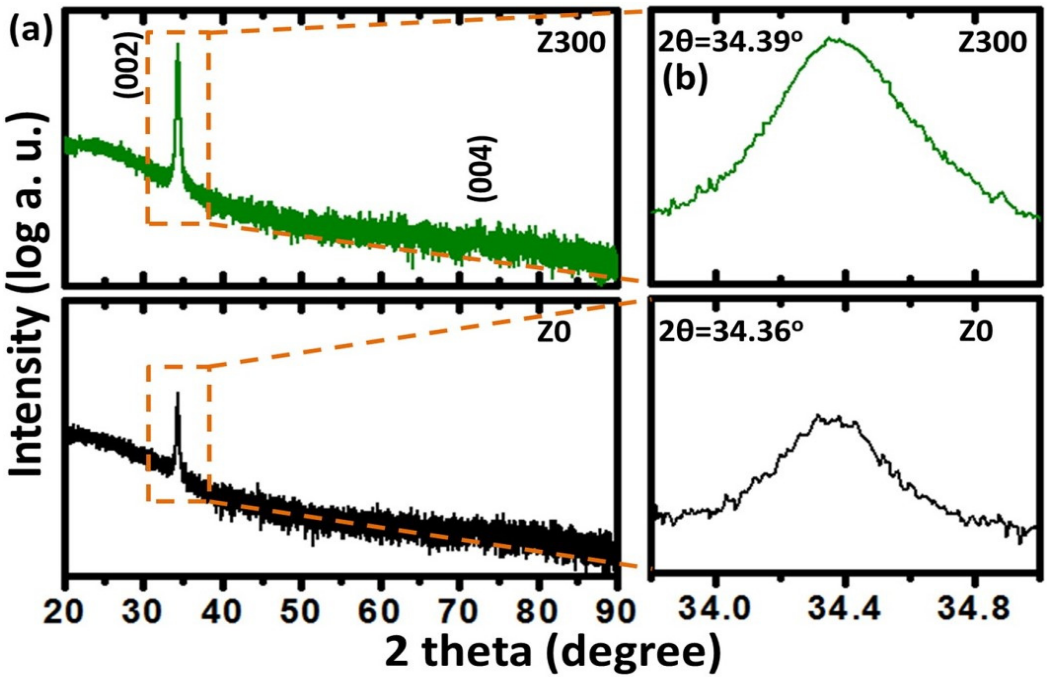

Figure 1. (a) X-ray diffraction spectra for the as-prepared ZnO films (Z0) and then have been modulated via a postannealing in vacuum furnace at 300°C for 30 *minutes* after deposition (Z300), respectively. (b) is the relating slow-scan spectra for the ZnO (002) diffraction peak in the θ-2θ region of (a).

For the purpose of confirming the internal stress between these two samples, the internal stress σ of hexagonal/ wurtzite crystal structure materials can be illustrated as:

$$\sigma = 450(c\text{-}c_0)/c_0 \text{ GPa} \quad (1)$$

where c is the lattice *parameter*/ constant for c-axis of hexagonal crystal structure that can be obtained from tough ZnO (002) peak originated from XRD patterns, and c_0 is 5.206 Å, the corresponding lattice constant value for bulk ZnO. As shown in Eq. (1), the lattice constant c_0 is used to calculate the internal stress of the textured ZnO compound. Furthermore, for the purpose of estimate the lattice constant, the Bragg's equation can be used for determining the lattice spacing of crystals.

$$n\lambda = 2d \sin\theta \quad (2)$$

In this case, where λ is the shortest wavelength of an incident X-rays (λ = 1.54 Å), and $d_{(002)}$ is for the interplanar spacing of hexagonal wurtzite structure of ZnO (002) facet. As shown in Figure 1, the ZnO (002) diffraction peak of both samples are located at 2θ = 34.36° and 34.39°, respectively. After substituting θ into Eq. (2), the $d_{(002)}$ of each sample is 2.607 Å and 2.605 Å, respectively. So based on above typical definitions, it can be calculated the c-axis lattice constant of ZnO from the above obtained results. Therefore, the value of lattice constant for each sample is 5.214 Å and 5.21 Å, respectively. At last, replacing each lattice constant into Eq. (1), and then the internal stress for textured ZnO films could be calculated and obtained. As shown in Figure 2, the internal stress of samples Z0 and Z300 were be calculated by the obtained information from X-ray diffraction spectra, and the calculated values of internal stress for samples Z0 and Z300 are -0.76 GPa and -0.46 GPa, respectively. Apparently, the values of internal stress for Z0 and Z300 are indeed modulated by a simple postannealing modification. According to the obtained results above, the internal stress of textured ZnO films was modulated via a suitable postannealing temperature and time, hence this kind of transition was attributed to the much higher heat energy during the postannealing modification. So the energetic particles bombardment and the design of heterostructured films could be applied into the laxation of internal stress and accompanied by the transition of grain-size morphology [47,48].

Preprints (www.preprints.org) | NOT PEER-REVIEWED | Posted: 12 July 2023 doi:10.20944/preprints202307.0833.v1

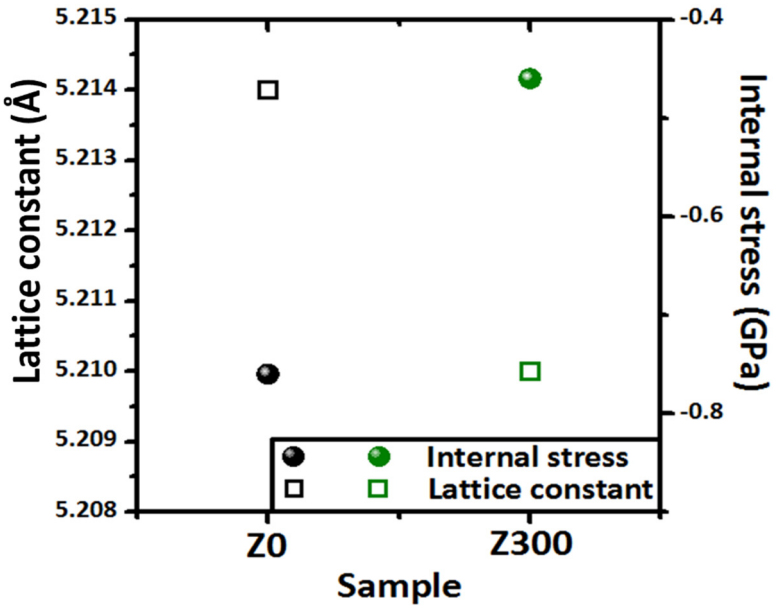

Figure 2. The relationship between lattice *parameter*/ constant and internal stress of samples Z0 and Z300, respectively.

Meanwhile, the different internal stress will result in different microstructure, the plan-view SEM images for the as-prepared ZnO film and with postannealing modification at 300°C as shown in Figures 3a,b. Figures 3a,b display modulable grain microstructures accompanied by a change in grain size corresponding to samples Z0 and Z300, respectively. This kind of grain size transition was induced by a postannealing modification that can be easily manipulated. The as-prepared ZnO film (Z0) with the average grain size is 29 ± 2 nm as displayed in the inset of Figure 3a. In addition, the ZnO film via a postannealing modification at 300°C (Z300) with average grain size is 53 ± 2 nm as shown in the inset of Figure 3b. The grain size histograms for fractions and distribution analysis *by using Gaussian* mode fitting curve (red line) are shown in the inset of Figures 3a,b. Such kind of improvement could be contributed to getting much higher heat energy during the postannealing modification that directly leading to the enhancement of grain growth kinetics, and the microstructure of the ZnO films could be modulated via the varied temperature and time of postannealing modification. That could be known via a postannealing modification, the nanograin with complex domain amalgamate and combine with each other to develop grain coalescence as displayed in Figure 3b. It can also be examined that the apertures located between grain and grain can catch oxygen inside and exist onto the surface area of top film. The corresponding images of water droplet on the ZnO surfaces are displayed in Figures 3c,d. The surface water contact angles (CAs) are 95° and 68° for samples Z0 and Z300, respectively. The as-prepared ZnO film shows hydrophobic wetting status due to the smaller nanograin size and much more apertures supply more the trapping of oxygen that decreases the contact area between water droplet and surface area of ZnO as displayed in Figure 3c. While with a postannealing modification at 300°C, the microstructure surface shows hydrophilic status, which is owning to the giant grain size and smooth surface, so it will get smaller apertures that cannot supply the trapping of oxygen between the interface of ZnO compound and the water droplet as shown in Figure 3d. This transformation caused the CA decreased from hydrophobic (CA = 95°) to hydrophilic (CA = 68°) status, and it was induced by the less apertures formed with a postannealing modification at 300°C. The schematic diagram is illustrating for the different modes showing the status of water droplet onto various surface structures of the ZnO compound as shown in Figure 3e. The microstructure contained smaller grains is with much more apertures and exhibits hydrophobic wetting status without any modification. In addition, the smooth surface with grain growth phenomenon leading to much less trapping of oxygen between the interface of ZnO compound and the water droplet, and then induced the wetting behavior from hydrophobic to hydrophilic status, which is to serve as a surface indication of grain

Preprints (www.preprints.org) | NOT PEER-REVIEWED | Posted: 12 July 2023 doi:10.20944/preprints202307.0833.v1

coalescence to form giant grain size. In short, the surface hydrophilicity could be promoted when there is less oxygen caught between the solid and liquid surface demonstrating a small CA via a simple factor of postannealing modification as schematically displayed in Figure 3e.

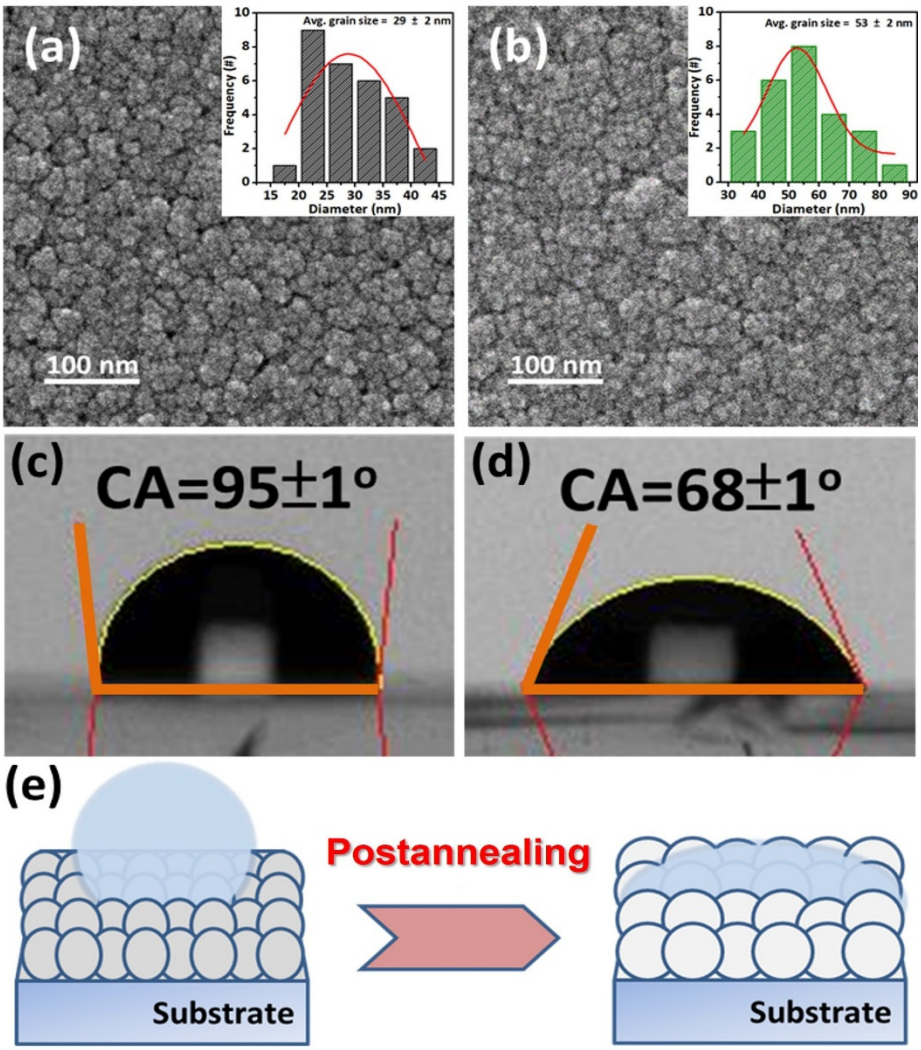

Figure 3. Plan-view FE-SEM images and the insets showed calculation of the average grain size and its distribution are for the prepared samples (a) Z0 and (b) Z300, respectively. (c) and (d) are for relating contact angle images for samples Z0 and Z300, respectively. (e) Schematic diagram is a transition of surface wetting behavior for ZnO samples without and with a postannealing modification.

Maintaining the high level of visible transmittance of device acts as a key role in the particular and industrial applications such as action wearable device and panel of the solar cell. Figure 4 shows the optical transparency for the as-prepared and with a postannealing modification of ZnO compound, respectively. From the spectra of optical transparency, the samples Z0 and Z300 exhibited highly transparent in the visible region with average transmittance values of 83.6% and 81.7%, respectively. The average transmittance of sample Z300 is slightly less than sample Z0, and it was attributed to the much more defect formation including mainly oxygen vacancies, which were formed while oxygen gas losing under vacuum atmosphere during a postannealing modification. From the above-mentioned results, all the highly textured ZnO films have excellent optical transparency and exhibit with a visible light transmittance beyond 80%. It is clearly displayed that both hydrophobic and hydrophilic surface wetting status of ZnO compound have potential to apply on smart window combined with the related optoelectronic, semiconducting and energy nanodevices.

Preprints (www.preprints.org) | NOT PEER-REVIEWED | Posted: 12 July 2023 doi:10.20944/preprints202307.0833.v1

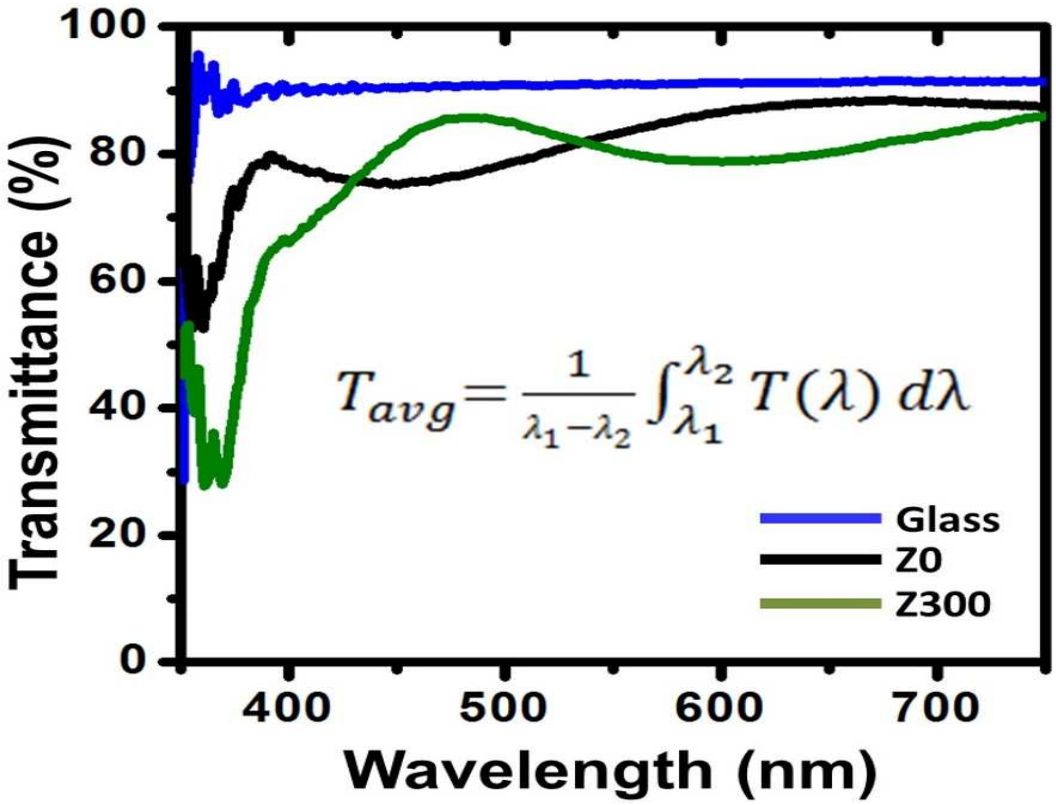

Figure 4. Transmittance spectra of the prepared samples Z0 and Z300 compared with pure glass substrate, respectively.

As a photonic material, it is important to verify the optical performance of ZnO compound, the photoluminescence (PL) spectra is considered as a regular method. Generally, it can be known that the PL emission spectrum of ZnO compound can be separated with two main sections. The first section belongs to near-band-edge (NBE) emission spectrum, which is contributed from the free-exciton recombination generating in UV zone. Another one is deep-level (DL) emission spectrum, which is constructed from the impurities and related possible defects mainly including oxygen vacancies and zinc interstitials that are originated from the suppression of the DL emission spectrum in visible zone. Figure 5 displays the PL spectra for both samples Z0 and Z300, respectively. The both samples demonstrate a tough NBE emission spectrum, which is positioned at approximately 374 nm and act for the dominant recombination mechanism of photogenerated charge carriers (excitonic photoemission). In contrast, another negligible defect band, which is positioned at approximately 546 nm (DL emission) induced by the intrinsic defects mainly including oxygen vacancies and zinc interstitials possibly existed in the ZnO compound, demonstrating that the ZnO compound are nearly defect-free. It is noteworthy that the tough peak of NBE emission spectrum for sample Z300 is slightly changed toward high wavelength band compared to the sample Z0. Based on previous published works, the peak shifting of NBE emission for the PL spectrum of ZnO in our present work can be induced by the quantum-size confinement effect [49–51]. On the other hand, the PL peak intensity in UV band of sample Z300 is slightly larger and narrower than the as-prepared sample Z0, which are related to the degree of crystallinity in the ZnO compound. In other words, it indicates that the PL spectra display an identical trend compared to the analysis results of XRD as both crystallinity and optical characteristics were simultaneously enhanced. Besides, the PL intensity of the peak in DL band with sample Z300 is slightly greater than the sample Z0 owning to the increasing oxygen vacancy while losing the oxygen atoms from the ZnO compound during a postannealing modification under the vacuum atmosphere.

Preprints (www.preprints.org) | NOT PEER-REVIEWED | Posted: 12 July 2023 doi:10.20944/preprints202307.0833.v1

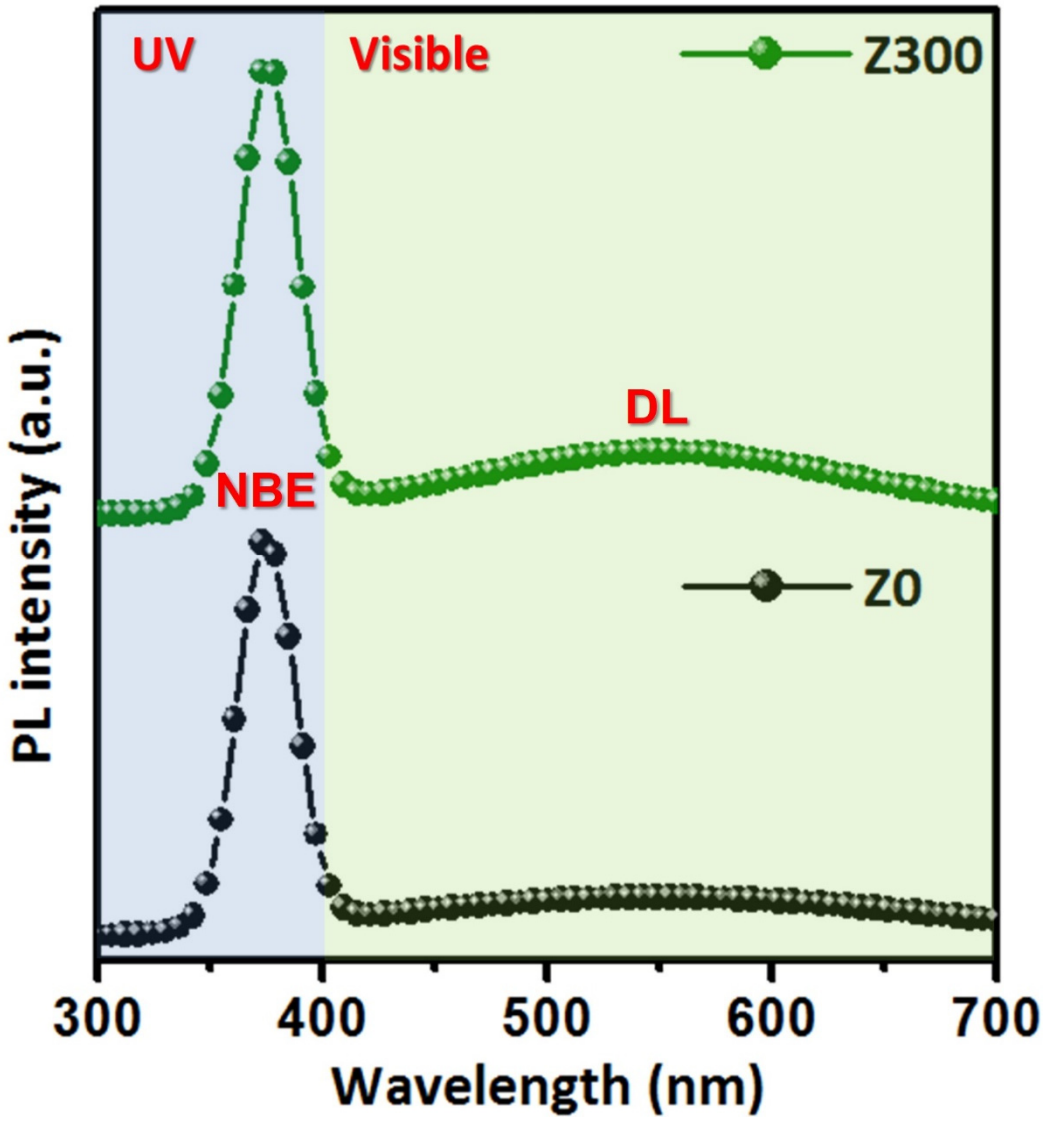

Figure 5. Photoluminescence spectra for the samples Z0 and Z300, respectively.

From the above-mentioned results, the highly textured ZnO prepared at RF power of 75 W without any postannealing modification shows the hydrophobic wetting behavior and the corresponding CA value is 95 ± 1°. However, the photocatalytic behavior has been widely reported and demonstrated by many works [52,53]. For the purpose of modulating the wetting behavior of the ZnO, the sample Z0 was placed under the ultraviolet (UV) light with a wavelength of 365 nm. This wavelength and strength of UV light has enough photon energy than the intrinsic band gap (3.37 eV) of the pristine ZnO. The relationship between the different powers of UV irradiation ranged from 330 to 3330 mW/cm^2 and the water contact angles (CAs) has been displayed in Figure 6. Figure 6 displays the related water CA images accompanied with the as-prepared ZnO compound (sample Z0), the drop of liquid water spread on the surface of sample Z0 with nanograin structure after UV irradiation for 10 min with different powers ranged from 330 to 3330 mW/cm^2. It can be clearly observed that the CA value of sample Z0 was reduced from 95±1° to 67±1° under the ultraviolet irradiation with 330 mW/cm^2 UV power. Moreover, the water CA value was highly reduced from 95 ± 1° to 49 ± 1° under the ultraviolet irradiation with 700 mW/cm^2 UV power. And then the water CA angles were dramatically drop-down from 95 ± 1° to 23 ± 1° and 19 ± 1° under the ultraviolet irradiation with 1520 and 3330 mW/cm^2 UV power, respectively. It demonstrates that the surface free energy of the ZnO compound was significantly modulated by the different power of ultraviolet irradiation and demonstrated the typical photocatalytic characteristics. In addition, the rapid reducement of CA values of as-prepared ZnO compound can be contributed from the photocatalytic reaction in ZnO

Preprints (www.preprints.org) | NOT PEER-REVIEWED | Posted: 12 July 2023 doi:10.20944/preprints202307.0833.v1

owning to the generating electron-hole pairs upon photoillumination induced by photoelectron emission. These holes and electrons can either recombine or change to the surface of semiconducting oxides to react with groups adsorbed on the surface of semiconducting oxides. Furthermore, when UV light irradiated on the ZnO compound and the generated photon energy equal or larger than the band gap of ZnO compound, the electrons (e^-) are excited into the conduction band from valence band. Simultaneously, the same number of holes (h^+) produced in valence band, some of the holes react with surface oxygen atoms or lattice oxygen (O^{2-}) to develop surface oxygen vacancies O^{1-}, while the electrons combine with lattice metal ions (Zn^{2+}) to develop Zn^{2+} defective sites, the water molecules and oxygen would contest with each other for the purpose of absorbing dissociatively on the imperfect sites. The surface status of semiconducting oxides caught electrons (Zn^+) toward to react with oxygen molecules adsorbed on the surface status of semiconducting oxides. In the meantime, the water molecules could coordinate with oxygen vacancy sits (V_O), which lead to the dissociative adsorption of the water molecules onto surface status of the ZnO semiconducting oxide. The imperfect sites are kinetically more desirable for hydrophilic adsorption of hydroxyl groups (OH^-) than adsorption of oxygen molecules.

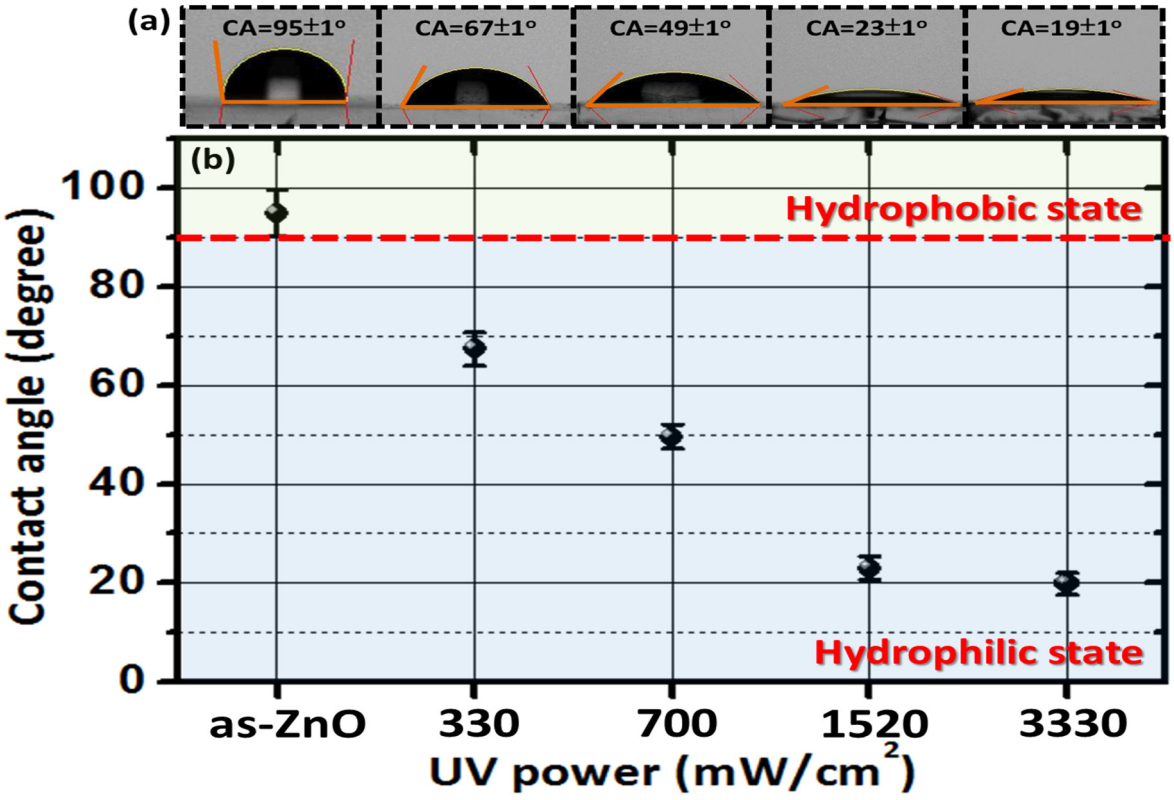

Figure 6. (a) The contact angle (CA) images for the sample Z0 under UV irradiation for 10 min without and with the different UV powers ranged from 330 to 3330 mW/cm², respectively. (b) The UV power as a function of CA value for sample Z0 under UV irradiation with a light wavelength of 365 nm.

Preprints (www.preprints.org) | NOT PEER-REVIEWED | Posted: 12 July 2023 doi:10.20944/preprints202307.0833.v1

In addition, the Eqs. (3-7) depict that the photocatalytic mechanism of imperfect sites on surface of ZnO semiconducting oxide.

$$ZnO + 2h\nu \rightarrow 2h^{+} + 2e^{-} \quad (3)$$

Some of surface oxygen atoms or lattice oxygen (O^{2-}) react with the holes to generate surface oxygen vacancies O^{1-}, while some of the lattice metal ions (Zn^{2+}) react with electrons to generate Zn^{2+} imperfect sites, as depicted in the subsequent equations.

$$O^{2-} + h^{+} \rightarrow O^{1-} \text{ (surface hole trapping)} \quad (4)$$

$$Zn^{2+} + e^{-} \rightarrow Zn^{+} \text{ (surface electron trapping)} \quad (5)$$

$$O^{1-} + h^{+} \rightarrow 1/2O_2 \text{ (gas)} + V_O \text{ (surface oxygen vacancies)} \quad (6)$$

The oxygen and water molecules could contest with each other to absorb dissociatively on the imperfect sites. The surface caught electrons (Zn+) toward to react with oxygen molecules adsorbed on the ZnO surface of semiconducting oxide:

$$Zn + O_2 \rightarrow Zn^{2+} + O^{2-} \quad (7)$$

An UV irradiation can modulate the chemical surface states of the ZnO semiconducting oxide, and therefore manipulated its surface wetting behavior. From the above-mentioned results, the surface wetting behavior can be simply modulated by a simple factor such as *power* of UV irradiation. Besides those mentioned ZnO, it is considered as a candidate with many potential devices such as biosensor, biomedical device and other multifunctional detecting devices [54–58].

The ZnO films was dispersed in methylene blue (MB) solution in order to measure the photocatalytic efficiency during UV irradiation in 10 min steps as shown in Figure 7. The photodegradation rate (K) of ZnO films can be calculated as the following equation (8):

$$-\ln\left(\frac{C}{C_0}\right) = Kt \quad (8)$$

where C_0 is the UV-Vis absorbance of the solution before irradiation (initial MB concentration), C is the UV-Vis absorbance of the solution after irradiation (concentration of MB at time t), K is the apparent rate coefficient (kinetic degradation rate), and t is reaction time of catalysts.

The photodegradation ratios of the MB solution with and without ZnO films (C/C_0) versus exposure/ reaction time (t) under UV light are shown in Figure 7(a). The examination in the absence of photocatalyst shows an insignificant photocatalytic efficiency of MB, indicating an insignificant self-photolysis of MB molecules under the illumination of UV light. C_0 is the initial concentration of MB and C is the MB concentration varied during the exposure time of UV light irradiation. The value of C/C_0 for solution with ZnO films is decreased with increasing the exposure time of UV light irradiation, so C/C_0 is simply calculated as the ratio between these photoabsorbance values. Figure 7(a) shows that pure ZnO film is useful as the photocatalysts with enough photocatalytic efficiency. The linear relationship of $-\ln(C/C_0)$ as a function of reaction time is plotted in Figure 7(b), and the apparent rate coefficient (K) for MB photodegradation is evaluated via the pseudo-first-order approximation, which is proportional to the corresponding values of photoabsorbance. The photodegradation rate (K) is calculated as the slope of the linear fit in $\ln(C/C_0)$ versus t plot for each sample, and the kinetic degradation rate (K) for pure ZnO film is equal to 2.93×10^{-3} (min^{-1}). Therefore, the general principle of dye-sensitized photocatalytic reaction related to ZnO film for MB solution is plotted in Figure 7.

Preprints (www.preprints.org) | NOT PEER-REVIEWED | Posted: 12 July 2023 doi:10.20944/preprints202307.0833.v1

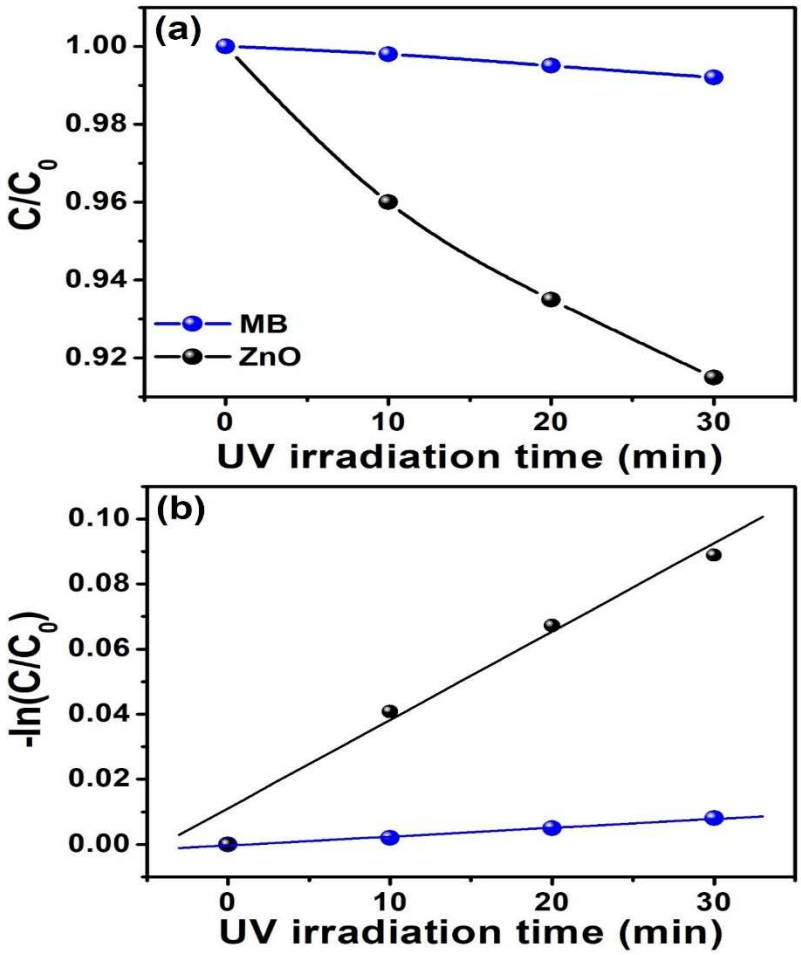

Figure 7. (a) (C/C_0) and (b) $-\ln(C/C_0)$ ratios as a function of reaction time for photocatalytic degradation of MB solution in the presence of the ZnO film under UV irradiation.

When absorption of energy is higher than the band gap energy of the ZnO, the holes (h^{+}_{VB}) are generated in valence band (VB) and electrons (e^{-}_{CB}) in conduction band (CB), respectively. This phenomenon was directly related to the existence of superficial ZnO lattice oxygen atoms/ ions that can associate with the oxidation of the adsorbed MB molecules, leading to the existence of surface hydroxyl groups acting as hole-acceptors to generate OH· radicals, which can be responsible for the generation of superoxide ions [59–64]. So the hydroxyl radicals (· 0H) decompose the MB effectively to generate water (H_2O), carbon dioxide (CO_2), and other inorganic by-products.

To further investigate the plasmonic coupling effect, a 15 nm thick Pt nanolayer was selected to deposit onto ZnO compound by direct-current (dc) **sputtering**, which was denoted as Pt/ZnO. A Pt thin film was existed with continuous layered structure deposited onto ZnO semiconducting oxide as observed by the two-dimensional (2D) AFM topographical morphology as displayed in Figure 8a. The continuous growth of capping nanolayer is also supported by three-dimensional (3D) AFM micrograph as displayed in Figure 8b. From AFM line-scan as displayed in Figure 8c, the height of Pt continuous structure was observed. The plan-view SEM image of Pt/ZnO heterostructures showed highly uniform state, and typically displayed flat surface morphology as displayed in Figure 8d. It can be obviously observed that the CA value of Pt/ZnO heterostructures was changed from 95 ± 1° (ZnO) to 86 ± 1° (Pt/ZnO) while capping with a Pt continuous nanolayer as displayed in Figure 8e. The X-ray scattering was used to ideally complement these microscopic methods since it could successfully reflect representative microstructural information for a large sample area for Pt/ZnO heterostructured films as displayed in Figure 8f. The XRD pattern for Pt/ZnO heterostructured films has typical ZnO(002) and Pt(111) diffraction peaks, which supports the existence of Pt nanolayer coated onto ZnO semiconducting oxide, which can be indexed to Pt/ZnO bilayer films in a crystalline phase. In addition, there is no diffraction peak of indefinite phase from Pt/ZnO bilayer films was

Preprints (www.preprints.org) | NOT PEER-REVIEWED | Posted: 12 July 2023 doi:10.20944/preprints202307.0833.v1

obtained, thus suppling strong proof for complete coverage of the ZnO by Pt without an intermixed phase. Above structural and morphological data analysis support the configuration of Pt/ZnO heterostructured films, and the XRD spectra analysis is consisted with the observation from the topical AFM and SEM images as displayed in Figure 8.

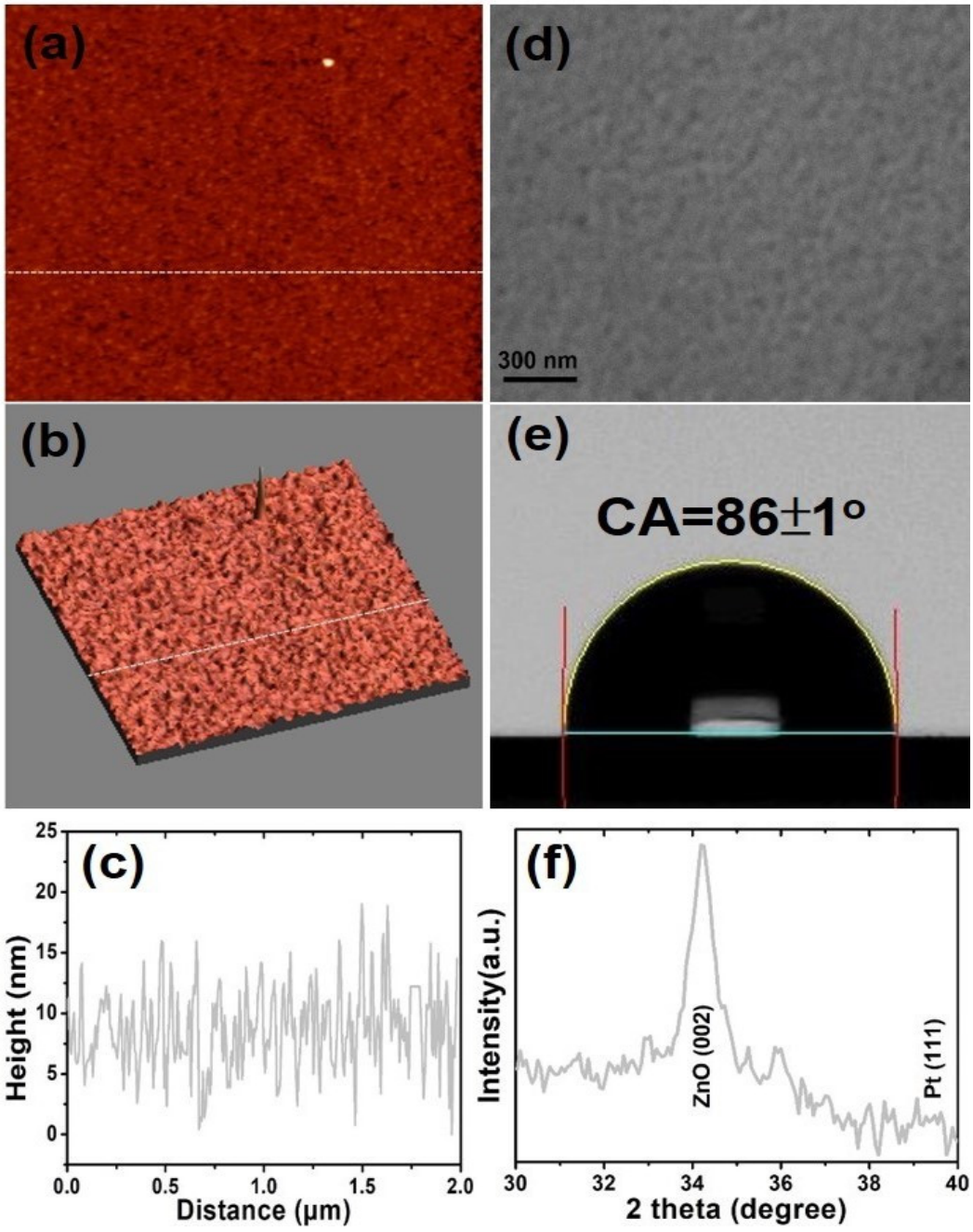

Figure 8. AFM topographical morphology of the Pt/ZnO bilayer films (a) 2D topical feature; (b) is 3D feature for (a), and (c) is a line scan profile of Pt/ZnO bilayer films related to (a) and (b), and the scan area is 2 × 2 μm². (d) is a plan-view SEM micrograph. (e) is a CA image. (f) is a corresponding x-ray diffraction pattern.

In addition, the surface plasmonic resonance (SPR) is coupled electron and photon oscillations that can be obtained and generated at the interface between Pt metal and ZnO semiconductor for the purpose of designing SPR heterostructures. Usually the pure metals could offer surface plasmonic collective oscillations of free electrons, which could collect the electromagnetic (EM) waves to a little fraction of a wavelength while enhancement of local field energy by several times of magnitude [65].

Preprints (www.preprints.org) | NOT PEER-REVIEWED | Posted: 12 July 2023 doi:10.20944/preprints202307.0833.v1

It was reported that the local EM field experienced by analyte molecules on the metal surface in nanoscale is dramatically enhanced, generating considerably enhanced Raman intensity [66]. We considered such kind of ZnO semiconductor capped with a continuous Pt nanolayer with suitable thickness which could induce localized field around its surface, there may be a coupling effect and exhibit the SPR. For the purpose of confirming this idea, the Raman spectra of the pristine ZnO and Pt/ZnO bilayer heterostructures were measured at room temperature as shown in Figure 9. In the case of Pt/ZnO heterostructured films exhibited a remarkable peak enhancement, the frequency of 1LO phonon peak is positioned at approximately 573 cm^{-1} corresponded to A_1 (LO) phonon, while the E_1 (TO) mode is forbidden according to the Raman selection rule [67,68]. Thus, the absence of the TO mode in the measurements further confirms that the ZnO film is with highly *c*-axis orientation. Hence all the measured results inferred from X-ray diffraction patterns and Raman analysis show the same tendency.

The above result also demonstrates a surface-enhanced Raman scattering that can be obtained by capping with a Pt continuous nanolayer onto ZnO semiconducting oxide. Therefore, a simple method is achieved and presented here that the surface plasmonic resonance and surface wetting behavior of ZnO compound can be effectively modulated by capping a Pt continuous nanolayer not such as to decorate with metallic nanoparticles. The Pt/ZnO heterostructures exhibited many novel and valuable applications in future due to its multifunctional material characteristics acted as a typical structure of nanodevice design.

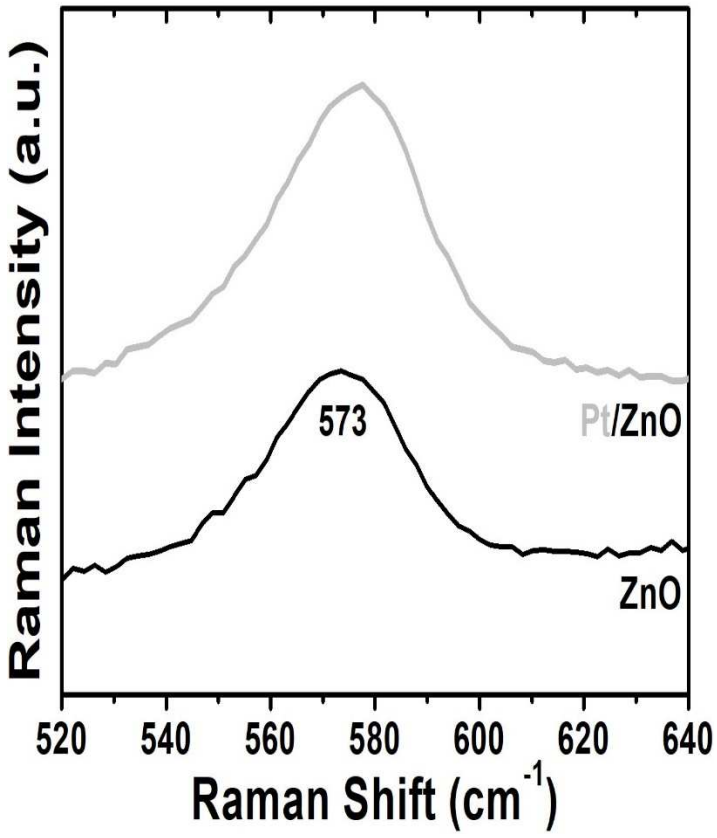

Figure 9. Raman spectra measured at room temperature for pristine ZnO semiconducting oxide without and with a Pt capping nanolayer.

4. Conclusions

In this work, the textured ZnO films were successfully prepared onto glass substrates with (002) orientation by radio-frequency magnetron sputtering system without supplying oxygen source at room temperature, and even epitaxial ZnO (004) facet can be obtained via a postannealing modification at 300°C. All the ZnO semiconducting oxide demonstrated excellent crystallinity and

Preprints (www.preprints.org) | NOT PEER-REVIEWED | Posted: 12 July 2023 doi:10.20944/preprints202307.0833.v1

high level of visible transmittance (beyond 80%). The as-prepared ZnO semiconducting oxide displayed the hydrophobic status, and then even transfer to hydrophilic status via a simple postannealing modification. The CA value, internal stress and the optical transmittance of photoluminescence for ZnO semiconducting oxide were significantly modulated by the surface microstructure, which is induced by a simple factor of postannealing modification. The rapid CA conversion of the ZnO semiconducting oxide could be modulated from hydrophobic (95°) to superhydrophilic (19°) by using a simple method via different power of UV light irradiation. The rapid transformation of CA for ZnO semiconducting oxide is due to the photocatalytic reaction induced by the positive surface charges accumulated on the surface via photoelectron emission. A greater impact on photocatalytic efficiency of ZnO film for the MB degradation is confirmed. Therefore, a simple way is proposed herein that the CA and photocatalytic variation of ZnO compound can be easily modulated by postannealing modification and ultraviolet irradiation, respectively. The enhanced Raman intensity in the Pt/ZnO bilayer heterostructures could be obtained due to the strong coupling of the light emission with the localized surface plasmonic resonance of the Pt nanolayer that could offer an effective path to lead more photonic scattering from incident light and further be used for sensing and multifunctional nanodevices design of wearable technologies.

Author Contributions: Conceptualization, Wei, D.-H.; methodology, Wei, D.-H.; software, Wei, D.-H., Tong, S.-K., and Chen, S.-C.; validation, Wei, D.-H.; formal analysis, Wei, D.-H.; investigation, Wei, D.-H.; resources, Wei, D.-H. and Hang, R.-T.; data curation, Wei, D.-H. and Chen, S.-C.; writing—original draft preparation, Wei, D.-H.; writing—review and editing, Wei, D.-H; visualization, Wei, D.-H.; supervision, Wei, D.-H.; project administration, Wei, D.-H. and Hang, R.-T.; funding acquisition, Wei, D.-H. and Hang, R.-T. All authors have read and agreed to the published version of the manuscript.

Funding: This research was funded by the National Science and Technology Council (NSTC) through Grants numbered 111-2731-M-027-001 and 112-2221-E-027-111 and the University System of Taipei Joint Research Program through Grant No. USTP-NTUT-NTOU-111-02. The authors acknowledge resources and support from the Quantum Materials Shared Facilities of Institute of Physics at Academia Sinica.

Institutional Review Board Statement: Not applicable.

Informed Consent Statement: Not applicable.

Data Availability Statement: Data are contained within the article.

Conflicts of Interest: The authors declare no conflicts of interest.

References

1. Supin, K.K.; Namboothiri P M, P.; Vasundhara, M. Enhanced photocatalytic activity in ZnO nanoparticles developed using novel *Lepidagathis ananthapuramensis* leaf extract. *RSC Adv.*, **2023**, 13, 1497–1515.
2. Zhao, F.; Lin, J.; Lei, Z.; Yi, Z.; Qin, F.; Zhang, J.; Liu, L.; Wu, X.; Yang, W.; Wu, P. Realization of 18.97% theoretical efficiency of 0.9 μm thick c-Si/ZnO heterojunction ultrathin-film solar cells *via* surface plasmon resonance enhancement. ***Phys. Chem. Chem. Phys.***, **2022**, **24**, 4871–4880.
3. Mardosaitė, R.; Jurkevičūtė, A.; Račkauskas, S. Superhydrophobic ZnO Nanowires: Wettability Mechanisms and Functional Applications. *Cryst. Growth Des.*, **2021**, 21, 4765–4779.
4. Mei, G.; Menon, P.S.; Hegde, G. ZnO for performance enhancement of surface plasmon resonance biosensor: a review. *Mater. Res. Express*, **2020**, 7, 012003.
5. Cestellos-Blanco, Stefano.; Zhang, H.; Kim, J.M.; Shen, Y.X.; Yang, P. Photosynthetic semiconductor biohybrids for solar-driven biocatalysis. *Nat. Cata.* **2020**, 3, 245–255.
6. Gupta, A.K.; Hsu, C.H.; Chen, C.H.; Purwidyantri, A.; Prabowo, B.A.; Wang, J.L.; Tian, Y.C.; Lai, C.S. Au-spotted zinc oxide nano-hexagonrods structure for plasmon-photoluminescence sensor. *Sens. Actuator B-Chem.*, **2019**, 290, 100–109.
7. Prabowo, B.A.; Purwidyantri, A.; Liu, K.C. Surface plasmon resonance optical sensor: a review on light source technology. *Biosensors*, **2018**, 8, 80.
8. Kumar, A.; Dixit, T.; Palani, I.A.; Nakamura, D.; Higashihata, M.; Singh, V. Utilization of surface plasmon resonance of Au/Pt nanoparticles for highly photosensitive ZnO nanorods network based plasmon field effect transistor. *Physica E*, **2017**, 93, 97–104.
9. Wang, C.; Yang, H.W.; Tian, L.; Wang, S.Q.; Gao, N.; Zhang, W.L.; Wang, P.; Yin, X. P.; Li, G.T. Facile fabrication of highly controllable gating systems based on the combination of inverse opal structure and dynamic covalent chemistry. *Nanoscale*, **2017**, 9, 7268–7275.

Preprints (www.preprints.org) | NOT PEER-REVIEWED | Posted: 12 July 2023 doi:10.20944/preprints202307.0833.v1

10. Lai, Y.K.; Huang, J.Y.; Cui, Z.Q.; Ge, M.Z.; Zhang, K.Q.; Chen, Z.; Chi, L.F. Recent advances in TiO_2-based nanostructured surfaces with controllable wettability and adhesion. *Small*, **2016**, 12, 2203–2224.
11. Ma, Q.L.; Cheng, H.F.; Fane, A.G.; Wang, R.; Zhang, H. Recent development of advanced materials with special wettability for selective oil/water separation. *Small*, **2016**, 12, 2186–2202.
12. Ke, J.J.; Liu, Z.J.; Kang, C.F.; Lin, S.J.; He, J.H. Surface effect on resistive switching behaviors of ZnO. *Appl. Phys. Lett*. **2011**, 99, 192106.
13. Chi, P.W.; Wei, D.H.; Wu, S.H.; Chen, Y.Y.; Yao, Y.D. Photoluminescence and wettability control of NiFe/ZnO heterostructure bilayer films. *RSC Adv.*, **2015**, 5, 96705–96713.
14. Peng, K.Y.; Ho, Y.H.; Wei, D.H.; Yu, Y.C.; Yao, Y.D.; Tian, W.C.; Wei, P.K. Efficiency enhancement of organic light-emitting devices by using honeycomb metallic electrodes and two-dimensional photonic crystal arrays. *Organic Electronics*, **2014**, 15, 3043–3051.
15. Lin, C.A.; Tsai, D.S.; Chen, C.Y.; He, J.H. Significant enhancement of yellow–green light emission of ZnO nanorod arrays using Ag island films. *Nanoscale*, **2011**, 3, 1195–1199.
16. Chen, S.C.; Wei, D.H. Controlling Surface Wettability and Plasmonic Resonance of Au/ZnO Heterostructured Films. *J. Compos. Sci.* **2022**, 6, 328.
17. Wei, D.H.; Tong, S.K.; Chen, S.C.; Hao, Y.H.; Wu, M.R.; Yang, C.J.; Huang, R.T.; Chung, R.J. Tuning surface plasmonic resonance and surface wettability of Au/CrN films by nitrogen-containing gas, *Nanomaterials*, **2022**, *12*, 2575.
18. Li, Q.; Meng, J.; Huang, J.; Li, Z. Plasmon-Induced Pyro-Phototronic Effect Enhancement in Self-Powered UV–Vis Detection with a ZnO/CuO p–n Junction Device. *Adv. Funct. Mater.*, **2021**, 32, 2108903.
19. Wei, D.H.; Lin, T.K.; Liang, Y.C.; Chang, H.W. Formation and Application of Core-Shell of FePt-Au Magnetic-Plasmonic Nanoparticles. *Front. Chem.*, **2021**, 9, 653718.
20. Pan, K.Y.; Wei, D.H. Optoelectronic and electrochemical properties of vanadium pentoxide synthesized by vapor-solid process. *Nanomaterials*, **2016**, 6, 140.
21. Chen, X.Q.; Wu, Z.S.; Liu, D.D.; Gao, Z.Z. Preparation of ZnO photocatalyst for the efficient and rapid photocatalytic degradation of azo dyes. *Nanoscale Res. Lett.*, **2017**, 12, 143.
22. Zhao, D.F.; Jia, R.; Gao, N.K.; Yan, W.S.; Zhang, L.; Li, X.; Liu, D. Near-infrared promoted wettability recovery of superhydrophilic ZnO. *J. Phys. Chem. C*, **2017**, 121, 12745–12749.
23. Zhang, B.Y.; Lu, S.X.; Xu, W.G.; Cheng, Y.Y. Controllable wettability and morphology of electrodeposited surfaces on zinc substrates. *Appl. Surf. Sci.*, **2016**, 360, 904–914.
24. Li, J.; Jing, Z.J.; Yang, Y.X.; Zha, F.; Yan, L.; Lei, Z.Q. Reversible low adhesive to high adhesive superhydrophobicity transition on ZnO nanoparticle surfaces, *Appl. Surf. Sci.*, **2014**, 289, 1–5.
25. Li, H.; Zheng, M.J.; Liu, S.D.; Ma, L.; Zhu, C.Q.; Xiong, Z.Z. Reversible surface wettability transition between superhydrophobicity and superhydrophilicity on hierarchical micro/nanostructure ZnO mesh films. *Surf. Coat. Technol.*, **2013**, 224, 88–92.
26. Xu, C.L.; Fang, L.; Wu, F.; Huang, Q.L.; Yin, B. Wetting behavior of triethoxyoctylsilane modified ZnO nanowire films. *Colloid Surf. A-Physicochem. Eng. Asp.*, **2014**, 444, 48–53.
27. Myint, M.T. Z.; Kumar, N.S.; Hornyak, G.L.; Dutta, J. Hydrophobic/hydrophilic switching on zinc oxide micro-textured surface. *Appl. Surf. Sci.*, **2013**, 264, 344–348.
28. Huang, Z.Y.; Luo, P.; Chen, W.Z.; Pan, S.R.; Chen, D.H. Hemocompatibility of ZnO thin films prepared by filtered cathodic vacuum arc deposition. *Vacuum*, **2013**, 89, 220–224.
29. Liu, Y.; Lin, Z.Y.; Lin, W.; Moon, K.S.; Wong, C.P. Reversible superhydrophobic–superhydrophilic transition of ZnO nanorod/epoxy composite films. *ACS Appl. Mater. Interf.*, **2012**, 4, 3959–3964.
30. Chang, W.Y.; Lin, C.A.; He, J.H.; Wu, T.B. Resistive switching behaviors of ZnO nanorod layers, *Appl. Phys. Lett.* **2010**, 96, 242109.
31. Guo, L.; Zhang, H.; Zhao, D.X.; Li, B.H.; Zhang, Z.Z.; Jiang, M.M.; Shen, D.Z. High responsivity ZnO nanowires based UV detector fabricated by the dielectrophoresis method. *Sens. Actuator B-Chem.*, **2012**, 166-167, 12–16.
32. Jindal, K.; Tomar, M.; Gupta, V. Inducing electrocatalytic functionality in ZnO thin film by N doping to realize a third generation uric acid biosensor. *Biosens. Bioelectron.*, **2014**, 55, 57–65.
33. Chao, C.H.; Wei, D.H. Synthesis and Characterization of High c-Axis ZnO Thin Film by Plasma Enhanced Chemical Vapor Deposition System and Its UV Photodetector Application. *J. Vis. Exp.*, **2015**, 104, e53097.
34. Chao, C.H.; Weng, W.J.; Wei, D.H. Enhanced UV photodetector response and recovery times using a non-polar ZnO sensing layer. *J. Vac. Sci. Technol. A*, **2016**, 34, 02D106.
35. Munje, R.D.; Muthukumar, S.; Prasad, S. Lancet-free and label-free diagnostics of glucose in sweat using Zinc Oxide based flexible bioelectronics. *Sens. Actuator B-Chem.*, **2017**, 238, 482–490.
36. Chi, P.W.; Su, C.W.; Wei, D.H. Control of Hydrophobic Surface and Wetting States in Ultra-Flat ZnO Films by GLAD Method. *Appl. Surf. Sci.*, **2017**, 404, 380–387.
37. Chi, P.W.; Su, C.W.; Wei, D.H. Internal Stress Induced Natural Self-Chemisorption of ZnO Nanostructured Films. *Sci. Rep.*, **2017**, 7, 43281.

Preprints (www.preprints.org) | NOT PEER-REVIEWED | Posted: 12 July 2023 doi:10.20944/preprints202307.0833.v1

38. Navale, Y.H.; Navale, S.T.; Ramgir, N.S.; Stadler, F.J.; Gupta, S.K.; Aswal, D.K.; Patil, V.B. Zinc oxide hierarchical nanostructures as potential NO_2 sensors. *Sens. Actuator B-Chem.*, **2017**, 251, 551–563.
39. Rezaie, M.N.; Manavizadeh, N.; Abadi, E.M.N.; Nadimi, E.; Boroumand, F.A. Comparison study of transparent RF-sputtered ITO/AZO and ITO/ZnO bilayers for near UV-OLED applications. *Appl. Surf. Sci.*, **2017**, 392, 549–556.
40. Flickyngerova, S.; Netrvalova, M.; Novotny, I.; Bruncko, J.; Gaspierik, P.; Sutta, P.; Tvarozek, V. Ion sputter etching of ZnO:Ga thin film surfaces. *Vacuum*, **2012**, 86, 703–706.
41. Quan, Z.Y.; Liu, X.; Qi, Y.; Song, Z.L.; Qi, S.F.; Zhou, G.W.; Xu, X.H. Robust room temperature ferromagnetism and band gap tuning in nonmagnetic Mg doped ZnO films. *Appl. Surf. Sci.*, **2017**, 399, 751–757.
42. Opel, M.; Geprägs, S.; Althammer, M.; Brenninger, T.; Gross, R. Laser molecular beam epitaxy of ZnO thin films and heterostructures. *J. Phys. D: Appl. Phys.*, **2014**, 47, 034002.
43. Alema, F.; Ledyaev, O.; Miller, R.; Beletsky,V.; Osinsky, A.; Schoenfeld, W.V. Growth of high Mg content wurtzite MgZnO epitaxial films via pulsed metal organic chemical vapor deposition. *J. Cryst. Growth*, **2016**, 435, 6–11.
44. Montero, M.M.; Borras, A.; Saghi, Z.; Espinos, J.P.; Barranco, A.; Cotrino, J.; Elipe, A.R.G. Vertical and tilted Ag-NPs@ZnO nanorods by plasma-enhanced chemical vapor deposition. *Nanotechnology*, **2012**, 23, 255303.
45. Chao, C.H.; Wei, D.H. Growth of Non-Polar ZnO Thin Films with Different Working Pressures by Plasma Enhanced Chemical Vapor Deposition. *Jpn. J. Appl. Phys.*, **2014**, 53, 11RA05.
46. Chao, C.H.; Chi, P.W.; Wei, D.H. Investigations on the crystallographic orientation induced surface morphology evolution of ZnO thin films and their wettability and conductivity. *J. Phys. Chem. C*, **2016**, 120, 8210–8219.
47. Chi, P.W.; Wei, D.H.; Yu, C.C.; Yao, Y.D. Magnetic-control-electric and reversal behavior of ZnO/NiFe/ZnO multilayer films. *AIP Adv.*, **2017**, 7, 056309.
48. Chi, P.W.; Wei, D.H. Dielectric Enhancement with Low Dielectric Loss in Textured ZnO Films Inserted with NiFe. *J. Mater. Chem. C*, **2017**, 5, 1394–1401.
49. Makhal, A.; Sarkar, S.; Bora, T.; Baruah, S.; Dutta, J.; Raychaudhuri, A.K.; Pal, S.K. Role of resonance energy transfer in light harvesting of zinc oxide-based dye-sensitized solar cells. *J. Phys. Chem. C*, **2010**, 114, 10390–10395.
50. Layek, A.; De, S.; Thorat, R.; Chowdhury, A. Spectrally resolved photoluminescence imaging of ZnO nanocrystals at single-particle levels, *J. Phys. Chem. Lett.*, **2011**, 2, 1241–1247.
51. Wang, N.W.; Yang, Y.H.; Yang, G.W. Great blue-shift of luminescence of ZnO nanoparticle array constructed from ZnO quantum dots. *Nanoscale Res. Lett.*, **2011**, 6, 338.
52. Rudakova, A.V.; Oparicheva, U.G.; Grishina, A.E.; Maevskaya, M.V.; Emeline, A.V.; Bahnemann, D.W. Dependences of ZnO photoinduced hydrophilic conversion on light intensity and wavelengths. *J. Phys. Chem. C*, **2015**, 119, 9824–9828.
53. Bai, X.J.; Wang, L.; Zong, R.L.; Lv, Y.H.; Sun, Y.Q.; Zhu, Y.F. Performance enhancement of ZnO photocatalyst via synergic effect of surface oxygen defect and graphene hybridization. *Langmuir*, **2013**, 29, 3097–3105.
54. Choi, A.; Kim, K.; Jung, H.I.; Lee, S.Y. ZnO nanowire biosensors for detection of biomolecular interactions in enhancement mode. *Sens. Actuator B-Chem.*, **2010**, 148, 577–582.
55. Ma, Y.Y.; Din, H.; Xiong, H.M. Folic acid functionalized ZnO quantum dots for targeted cancer cell imaging. *Nanotechnology*, **2015**, 26, 305702.
56. Mohammed, A.M.; Ibraheem, I.J.; Obaid, A.S.; Bououdina, M. Nanostructured ZnO-based biosensor: DNA immobilization and hybridization. *Sens. Bio-Sens. Res.*, **2017**, 15, 46–52.
57. Tripathy, N.; Kim, D.H. Metal oxide modified ZnO nanomaterials for biosensor applications. *Nano Converg.*, **2018**, *5*, 27.
58. Swaminathan, N.; Sharma, N.; Nerthigan, Y.; Wu, H.F. Self-assembled diphenylalanine-zinc oxide hybrid nanostructures as a highly selective luminescent biosensor for trypsin detection. *Appl. Surf. Sci.*, **2021**, 554, 149600.
59. Chen, C.; Ma, W.; Zhao, J. Semiconductor-mediated photodegradation of pollutants under visible-light irradiation. *Chem. Soc. Rev.*, **2010**, 39, 4206–4219.
60. Chen, K H.; Pu, Y.C.; Chang, K.D.; Liang, Y.F.; Liu, C.M.; Yeh, J.W.; Shih, H.C.; Hsu, Y.J. Ag-Nanoparticle-Decorated SiO_2 Nanospheres Exhibiting Remarkable Plasmon-Mediated Photocatalytic Properties, *J. Phys. Chem. C* **2012**, 116, 19039.
61. Ahmad, H.; Kamarudin, S.K.; Minggu, L.J.; Kassim, M. Hydrogen from photo-catalytic water splitting process: A review, *Renewable and Sustainable Energy Reviews* **2015**, 43, 599–610.
62. Kadi, M.W.; Kinney, D.M.; Mohamed, R.M.; Mkhalid, I.A.; Sigmund, W. Fluorine doped zinc oxide nanowires: Enhanced photocatalysts degrade malachite green dye under visible light conditions, *Ceram. Int.*, **2016**, 42, 4672–4678.

Preprints (www.preprints.org) | NOT PEER-REVIEWED | Posted: 12 July 2023 doi:10.20944/preprints202307.0833.v1

63. Chen, X.; Wu, Z.; Liu, D.; Gao, Z. Preparation of ZnO Photocatalyst for the Efficient and Rapid Photocatalytic Degradation of Azo Dyes, *Nanoscale Res. Lett.*, **2017**, 12, 143.
64. Blažeka, D.; Radičić, R. Maletić, D.; Živković, S. Momčilović, M.; Krstulović, N. Enhancement of Methylene Blue Photodegradation Rate Using Laser Synthesized Ag-Doped ZnO Nanoparticles, *Nanomaterials* **2022**, 12, 2677.
65. Giannini, V.; Fernnández-Domínguez, A. I.; Heck, S. C.; Maier, S. A. Plasmonic Nanoantennas: Fundamentals and Their Use in Controlling the Radiative Properties of Nanoemitters. *Chem. Rev.* **2011**, 111, 3888–3912.
66. Campion, A.; Kambhampati, P. Surface-Enhanced Raman Scattering. *Chem. Soc. Rev.*, **1998**, 27, 241–250.
67. Scott, J.F. UV resonant Raman scattering in ZnO. *Phys. Rev. B*, **1970**, 2, 1209–1211.
68. Alim, K.A.; Fonoberov, V.A.; Balandin, A.A. Origin of the optical phonon frequency shifts in ZnO quantum dots. *Appl. Phys. Lett.*, **2005**, 86, 053103.

Disclaimer/Publisher's Note: The statements, opinions and data contained in all publications are solely those of the individual author(s) and contributor(s) and not of MDPI and/or the editor(s). MDPI and/or the editor(s) disclaim responsibility for any injury to people or property resulting from any ideas, methods, instructions or products referred to in the content.